The Experiment of Flow Induced Vibration in PWR RCCAs

Sang-Nyung Kim*†, Cheol Shin
Department of Nuclear Engineering, Kyunghee University

Recently, severe wear on the shutdown rod cladding of Ulchin Nuclear Power Plant #1, #2 were observed by the Eddy Current Test(E.C.T.). In particular, the wear at the sixth card location was up to 75%. The test results indicated that the Flow Induced Vibration(F.I.V.) might be the cause of the fretting wear resulting from the contact between Rod Cluster Control Assemblies(RCCAs) and their spacing cards(guide plates) arranged in the guide tube. From reviewing RCCAs fretting wear reports and analyzing the general characteristics of F. I. V. mechanism in the reactor, geometric layout and flow conditions around the control rod, it is concluded that the turbulence excitation is the most probable vibration mechanism of RCCA. To identify the governing mechanism of RCCA vibration, an experiment was performed for a representative rod position in which the most serious fretting wear was experienced among the six rod positions. The experimental rig was designed and set up to satisfy the governing nondimensional numbers which are Reynolds number and mass damping parameter. The vibration amplitude measurement by the non-contact laser displacement sensor showed good agreements in the frequency and the maximum wearing(vibration) location with Ulchin E. C. T. results and Framatome report, respectively. The sudden increase in the vibration amplitude was sensed around the 6th guide plate with mass flow rate variation. Comparing the similitude rod behaviour with the idealized response of a cylinder in flow induced vibration, it was found that the dominant mechanism of vibration was transferred from turbulence excitation to periodic shedding at the mass flow rate 90l/min. Also the critical velocity of the vibration in RCCAs was determined and the vibration can be prevented by reducing the bypass flow rate below the critical velocity.

Key Words : Flow-Induced Vibration, F. I. V, Turbulent Excitation, Periodic Wake Shedding, PWR RCCAs, Control Rod

Nomenclature

a	: Rod radius
a_h	: Hydraulic radius of flow passage
C_f	: Frictional coefficient
c'	: Mechanical damping coefficient
D	: Diameter
D_e	: Equivalent diameter
EI	: Flexural rigidity
f	: Friction factor
f_n	: Natural frequency
F_a	: Lateral inviscid force
L	: Rod length
$\bar{M}$	: Total modal mass
ΔP	: Pressure drop
P	: Rodlets' pitch
U	: Flow velocity

Greeks

δ	: Logarithmic decrement of damping
ζ	: Dimensionless damping factor
η	: Dimensionless mass-damping parameter

† First Author
* Corresponding Author,
E-mail : snkim@nms.kyunghee.ac.kr
TEL : +82-31-201-2561 ; **FAX** : +82-31-202-1541
Department of Nuclear Engineering, Kyunghee University Seocheon-ri #1, Kiheung-up, Youngin-city,Kyunggi-do 449-701, Korea. (Manuscript **Recevied** January 14, 2000; **Revised** December 15, 2000)

ν : Lateral deflection of cylinder
ρ : Fluid density
$\phi_j(X)$: Eigenfunctions

Subscripts

c : Flow of center hole
r : Flow around control rod

Abbreviations

PWR : Pressurized Water Reactor
RCCAs : Rod Cluster Control Assemblies
E.C.T. : Eddy Current Test
F.I.V. : Flow Induced Vibration
EdF : Electricite de France
P.I.V. : Particle Image Velocimetry

1. Introduction

In the nuclear power plant, the integrity of the components is critically important not only for economic operation, but also for the plant safety. In 1986, however Framatome's RCCA cladding wear measurements in EdF plants indicated that excessive wear reaching 40% of its cladding occurred at some of their plants. The E. C. T. result of RCCAs of Ulchin #1, 2 plant also showed very serious state of wear reaching 77% at maximum (1995a, 1995b). Also there are some common features for RCCAs wearing pattern (Kim and Shin, 1998).

First, the fact that the RCCAs are all out during the normal operating period indicated the failure is irrelevant to the core. Second, the wear is localized at specific position, that is, the wear position coincides with the card position. Also, the wear is not longitudinal but lateral. Third, the amount of degradation is not exactly proportional to the operating time. Finally, the review result of wear pattern and distribution indicates that the vibration is the RCCAs' governing mechanism of the wear.

It also shows that the vibration can be related to the various plant factors like the geometry of the upper structures, flow distribution, RCCAs' position, and initial rodlet alignment in the guide tube. To understand the vibration mechanism in the complex guide tube, it is helpful to know

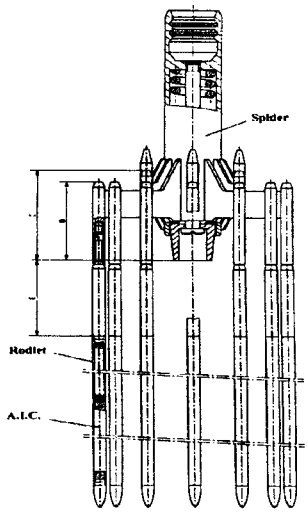

Fig. 1 RCCA spider diagram

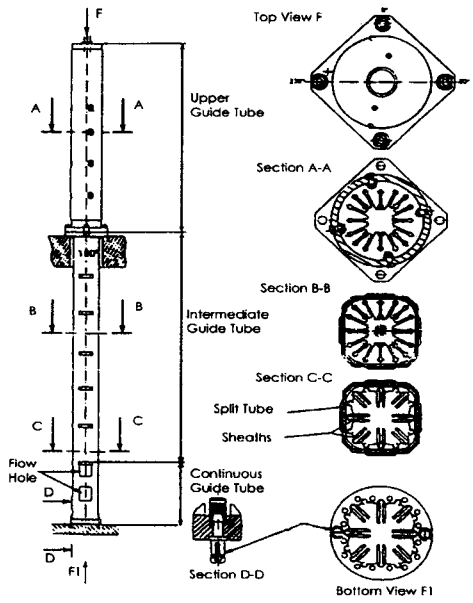

Fig. 2 RCCA guide tube and guide plate geometry along elevation

about its structure, geometry, and bypass flow through it.

In Ulchin Nuclear Power Plant #1, 2 and Framatome's plants which have 17×17 fuel assembly, RCCA has 24 rodlets brazed to a spider (Fig. 1) (Kim and Shin, 1998). The rodlet consists of a thin 304S. S. tube filled with a silver-indium-cadmium (Ag-In-Cd) cylindrical bar. The rod is long(3.8m), thin and very flexible.

Figure 2 shows a 17×17 RCCA guide tube. In the upper plenum locates the lower guide tube assembly, consisting of an enclosure with intermediate plates and a continuous support assembly used to guide and support the RCCA control rods. The lower guide tube assembly has a square cross-section member, and it is divided into intermediate and continuous assembly. The assembly is made up of sheaths and C-tube supports, so-called cards shown in the cross section C-C(Fig. 2). In the intermediate and upper guide tube, the guide plates are equipped but the continuous section has no guide plate except for its bottom and has some flow holes on its surface.

The upper head bypass flow injected into the upper plenum by spray nozzles around the periphery of the head exits the upper plenum by passing down through the guide tubes. All flow in the upper guide tube pass through the hole in the top housing plate, because the rest of the upper guide tube is impermeable. After passing through the upper core plate, some flow leak out from the intermediate guide plate sluts.

2. RCCAs' Wear Mechanism and Patterns

From analysing the Framatome's RCCA wear report (Leclercq, 1995) and the E. C. T. results of Ulchin plant #1, 2 (Kim and Shin, 1998), the common features of RCCA wear distribution are as follows.

A. The lower guide tube exit flow mainly affected the wear at the first plate above the continuous section for the inside rodlets.

B. The inside face(position E in Fig. 3) rodlet wear was the greatest, while the inside corner(F) rodlet wear was 40% to 65% as much, and the outer(A, B, C, D) rodlet wear was significantly lower(Fig. 4).

C. Misalignment of the plate resulted in localized lateral preloading which can dramatically increase the wear rate.

D. The most severe wear occurred on the intermediate flange plate No. 6.

However, these factors seem to affect very limited range of RCCAs' wear. More fundamentally

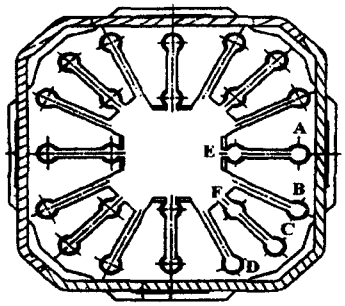

Fig. 3 Rodlet position in guide tube

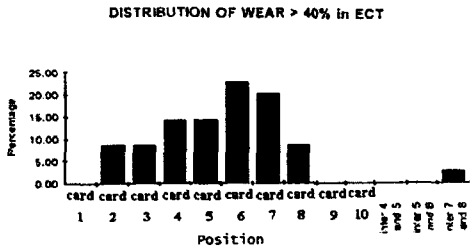

Fig. 4 The distribution of RCCA fretting wear in guide plate

affecting factor is the fluid force in the upper guide tube and damping coefficient of the control rod.

Based on these results, the major source of wear on the rodlets for the 17×17 design RCCA is primarily due to flow through the guide tube. With the consideration of flow conditions around the rodlets such as single(liquid) phase flow, axial tube flow and Reynolds number, the flow induced vibration may be caused by turbulent excitation or vortex shedding.

3. Mathematical Model of RCCA

An idealized and simplified analytical model was developed in this part to simulate the vibration of a portion of the rodlet between the guide tube plates. The first and last guide plates are presumed to provide positive support and are modeled as pinned ends. This assumption should not cause any error since the most severe vibration occurs at the 6th plate which is far from the end plate. No fluid forces through the plates are considered at these ends. The other plates are considered to provide no support and are modeled as a narrow annular passage, through

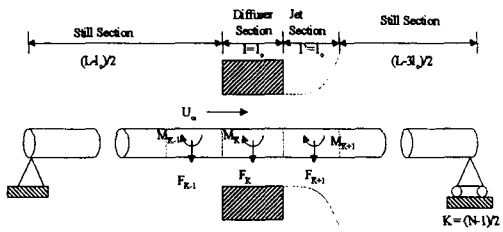

(a)

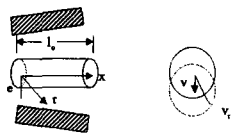

(b)

Fig. 5 (a) Diagram showing the annular flow passage (l) and the jet expansion zone (l') just downstream, (b) The cylindrical coordinate system used in the analysis

which all the flow in the neighborhood of the rodlet is funneled. The flow is essentially modeled as inviscid, although some aspects of viscosity are taken into account in a lumped form.

The system under consideration is shown in Fig. 5(a) and (b). There is an axial flow all along the rodlet. But over a small portion, the flow is forced to go through an annular passage at a much higher flow velocity. The cylinder is modeled as an Euler-Bernoulli beam with flexural rigidity EI, mass per unit length m, radius a, and length L ; then, denoting lateral deflections by v(X, t) the equation of motion may in general be written approximately, as follows (Yasuo and Paidoussis, 1989).

$$EI\frac{\partial^4 v}{\partial X^4}+F_a-\rho aU^2C_f(1+\frac{a}{a_h})(L-X)\frac{\partial^2 v}{\partial X^2}+\rho aU^2C_f(1+\frac{a}{a_h})\frac{\partial v}{\partial X}+(\rho aUC_f+c')\frac{\partial v}{\partial t}+m\frac{\partial^2 v}{\partial t^2}=0 \quad (1)$$

where C_f is a frictional coefficient, a_h the hydraulic radius of the flow passage, U the flow velocity, ρ the fluid density, F_a the lateral inviscid force, c' the mechanical damping coefficient, and v(X, t) is the lateral deflecton of cylinder.

It is assumed that the effect of flow-induced stiffness on the system is quite small, so that the third and fourth terms in Eq. (1) are neglected; then the flow-induced damping in the fifth term is lumped with c' to give an effective damping coefficient, c, which is presumed to also take into account the effect of squeeze-film damping in the narrow annulus, perhaps the most important source of damping of all. The solution of Eq. (1) can be assumed as follows.

$$v(X,\ t)=\sum_j \varphi_j(X)\,q_j(t),\ j=1,\ 2,\ \cdots \quad (2)$$

where, the comparison functions $\varphi_j(X)$ are the eigenfunctions of a pinned-pinned beam.

Eq. (1) then leads to

$$m\ddot{q}_j+c\dot{q}_j+(\frac{j\pi}{L})^4EIq_j=-\int_0^L F_a\varphi_j dX, \quad (3)$$

$$m\ddot{q}_1+c\dot{q}_1+(\frac{\pi}{L})^4EIq_1=\sum_{n=1}^{N}\varphi_1(X_n)F_N+\sum_{n=1}^{N}\varphi_1(X_n)M_N \quad (4)$$

$$F_n=F_n^2\frac{d^2}{dt^2}e^{\lambda t}+F_n^1\frac{d}{dt}e^{\lambda t}+F_n^0e^{\lambda t} \quad (5)$$

$$M_n=0 \quad (6)$$

where,

$$F_n^2\simeq -m_pv_n,\ F_n^1\simeq -m_p\{C_\beta U_ov_n+2U_o\psi_n\}$$
$$F_n^o\simeq -m_p\{[U_p+C_\beta U_o]U_o\psi_n-[U_0^2/EI]\Pi_n\}$$
$$m_p=\rho\pi a^2kl_o$$

Substituting Eqs. (5) and (6) into (4), the following expressions for the total modal mass, $\bar{M}$ are obtained

$$\bar{M}=m+(m_p/l_0k)\{1+2(k-1)(l_0/L)\} \quad (7)$$

and obtaining the dimensionless mass-damping parameter, $\eta=\frac{\bar{M}\delta}{\rho D^2}$, where, δ is the logarithmic decrement of damping (Yasuo and Paidoussis, 1989).

Most structures susceptible to flow-induced vibration are lightly damped, and the relationship between the dimensionless damping factor ζ, δ is $\zeta=\frac{\delta}{2\pi}$ (Blevins,)

4. Experimental Rig

The experimental rig was designed on the base of the governing nondimensional numbers which are mass, damping parameter and Renolds num-

ber. The correlation equation of the damping factor of the prototype rodlets is as follows.

$$\zeta=\frac{0.3267}{4\pi f_n}+5.80\times10^{-5}\pi f_n \quad (8)$$

The natural frequency of similitude rod is about 24Hz and the correlation equation of the damping factor is

$$\zeta=0.003+2.44\times10^{-4}U+3.44\times10^{-6}U^2 \quad (9)$$

The mass damping parameter of the prototype and the similitude rod are calculated as $\eta=\frac{\bar{M}\delta}{\rho D^2}\simeq0.3$ and each variable is presented in Table 1.

Table 1 The major factor computation of the dimensionless parameter

	Actual Control Rod	Model Rod
ζ	0.00611	0.00626
δ	0.0384	0.0393
f_n(Hz)	5	24
$\bar{M}$(g/cm)	6.49	12.3

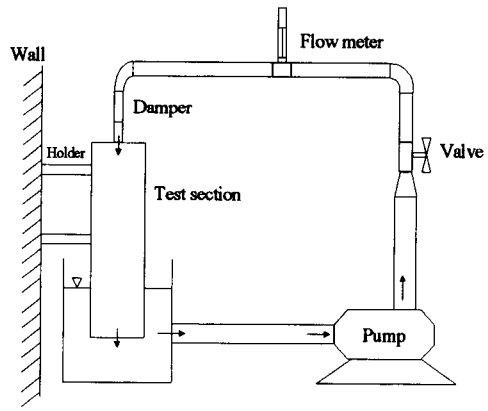

Fig. 6 Experimental rig schematic

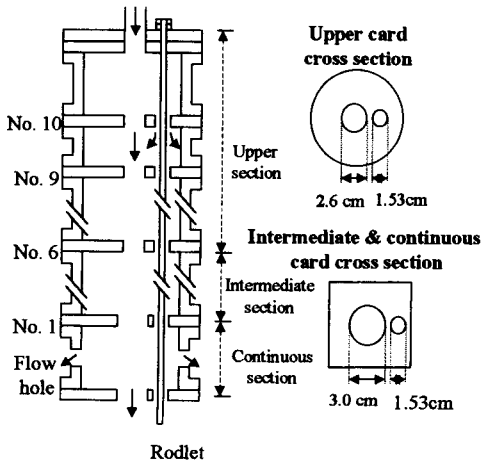

Fig. 7 Diagram of similitude guide tube and guide plate

Although a RCCA consists of 24 rodlets, experimental rig has only one representative rod. The prototype rodlets have very large pitch and diameter ratio(P/D) value and were hardly effected by the neighboring rods. Consequently, a single rod can represent all of the prototype rodlets (Paidoussis,). Also, to simulate the flow conditions around the rodlets, two flow paths are provided. One is large, and the other is small. The rodlet goes through the small path. The water passes through the gap between the rodlet and plate.

The rod was to simulate the rod of inside face position at which the maximum wear occurred out of the 6 positions.

The upper guide tube is impermeable, but the intermediate and the continuous guide tubes have some leakage flow. Considering the leakage flow, the center hole of the 6th plate is widened. The geometry of guide tube and plates were designed to satisfy the similitude law. A similitude brass rod (119 cm long, 1.27 cm diameter) was manufactured according to Chen et al's experimentl data(Wambsganss and Chen, 1971). The guide tube and plates were made of transparent acrylic plastic.

Non-contact laser vibrometer and digital oscil-

Table 2 The Specification of laser (CLV-700) sensor

Items	Features
Weight	500 g
Dimensions	228×48 mm
Laser output	<1mW, HeNe (633 nm) Laser safety class Ⅱ
Fiber cable	3 m to laser module (up to 10 m optical)
Laser spot size	45 μm@ 316 mm
Operating temp.	0-40 ℃

loscope were used to measure the real-time rod vibration. Table 2 shows the features of the laser sensor.

5. Experiment

Before carrying out the experiments the flow meter was calibrated by comparing the value of flow meter reading with the amount of water poured in the mass cylinder. The error range of the flow meter was about 5 %. Calibration for the laser sensor was conducted with a digital oscilloscope. However, many factors such as fines dust in air, pump noise, and the refraction caused by cylindrical transparent acrylic test section can bias the measurement. The signal uncertainty was minimized by spectrum analysis and filtering function which are built-in programs in the digital oscilloscope.

The interface between the data acquisition system and the test section is shown in Fig. 8. The laser from the sensor was transmitted through the cylindrical transparent acrylic test section and was reflected by the vibrating rod. The digital oscilloscope analyzes and records the phase difference, intensity, amplitude, etc.

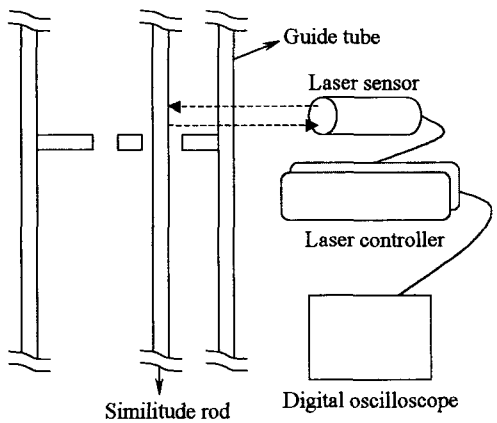

Fig. 8 Interface between data acquisition system and test section

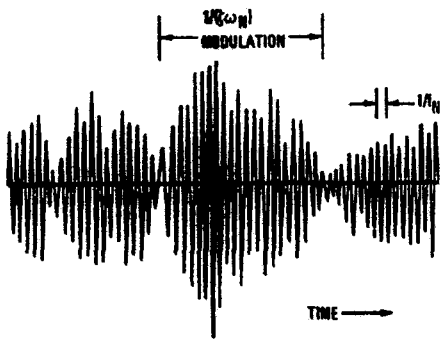

Fig. 9 Experiment data shape

The signal has a random shape and repeated module(Fig. 9). One module is equivalent to $\frac{1}{\zeta\omega_n}$ and the natural frequency, f_n of rod is calculated from the equation, $f_n=\frac{\omega_n}{2\pi}$.

The experiments were performed in two stages. The first stage experiment which concentrated on a fixed flow rate of 110*l*/min was executed to confirm the vibration displacement and frequency trend. The flow rate was selected based on the same Reynolds number of a real plant. The second stage experiment which concentrated on the 6th plate vibration was accomplished by changing the mass flow rate from 50*l*/min to 110*l*/min in 10*l*/min increments.

6. Results and Discussions

6.1 Results

The simulation experiment of control rod vibration was performed at room temperature and atmospheric pressure. Figure 10 shows the result of the first stage experiment which was performed to find out the most dominant vibration plate position and the vibration frequency at the fixed

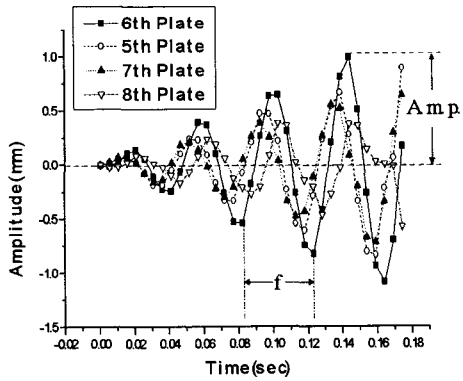

Fig. 10 The displacement variation for the most dominant four plates at fixed flow rate, 110 l/min (stage 1. exp.)

Table 3 Experiment matrix

Items \ Exp. No.	Stage 1	Stage 2
Interested points	Amplitude distribution with plates elevation	Amplitude variation with flow rate
Measured position	5th, 6th 7th, 8th plates	6th plate
Flow rate	110 *l*/min	50-110 *l*/min

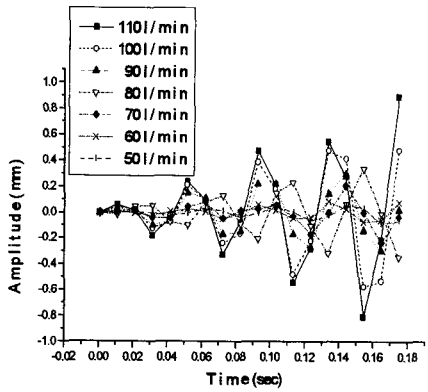

Fig. 11 The amplitude trend at 6th plate position with mass flow rate variation (stage 2. Exp.)

flow rate of 110*l*/min.

The results of the amplitude measurement along the plate position show that the largest amplitude occurred at the sixth plate. Also, the amplitude decreased as the distance from the sixth plate increased. Also the figure shows that the frequency of the vibration is 20 to 25 Hz since the period is about 0.05 sec. to 0.04 sec.

These measured results are exactly coincident with the Ulchin E. C. T. result and Framatome's report. This means that the design of the experimental rig, conditions, and method are quite adequate.

The results of the second stage experiment are shown in Fig. 11. The vibration amplitude steadily increases as the flow rate increases from 50*l*/min to 90*l*/min. After this steady increase stage, the amplitude increases drastically with the flow

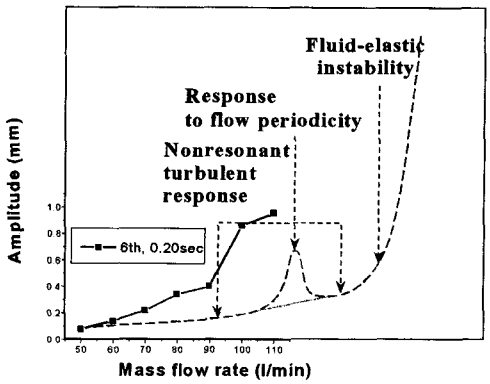

Fig. 12 Comparison of amplitude variation of similitude rod at the 6th plate with idealized response of single cylinder subjected to cross flow

rate. In this experiment(Fig. 7), the amplitude was limited to about 1 mm since the gap between the hole and rod is about 1 mm. To show this sudden amplitude increase in more detail, the results were redrawn in Figure 12. Figure 12 shows that the F. I. V. characteristic curve for an idealized rod matches that of the experimental results. Governing mechanisms are divided into three parts according to fluid velocity. Turbulent excitation mechanism is dominant in the low mass flow rate range, periodic wake shedding mechanism occurs at a certain velocity in the medium range, and fluid-elastic instability mechanism is essential in the high range. In the range from 50*l*/min to 90*l*/min, the amplitude increases with the mass flow rate gradually. But at the moment of changing mass flow rate from 90*l*/min to 100*l*/min, the amplitude increases dramatically. This behaviour of the amplitude can be explained as the transition of governing mechanism. Turbulent excitation is dominant in the low flow range (50-90*l*/min), then as the flow rate approaches 100*l*/min, the governing flow-induced vibration mechanism is changed to periodic wake shedding.

6.2 Discussions

The experimental results carried out with the experimental rig at atmospheric pressure and room temperature may be different from that of the actual plants by two factors. One is the pres-

sure and temperature effects and the other is the local flow velocity.

First the pressure and temperature effects will be discussed. The pressure effect on the rod vibration is negligible since the material properties of the control rod and liquid water would not significantly be changed by the pressure variation. However, the temperature variation would change the material properties of the control rod and water significantly. The most significant temperature effect on the water properties is the viscosity change which is already reflected by the Reynolds number at the design stage of the experimental rig. Also the control rod properties at high temperature were already reflected by the damping parameter at the design stage. Therefore, the temperature and pressure effects were already reflected on the experimental result.

The last one is the local flow velocity. In the experiment, the exact local velocity around the control rod was not measured. Therefore, the exact transition velocity from the turbulent excitation to wake shedding can not be determined. However, the approximate velocity can be found by the mass conservation for same pressure drop across the guide plate.

$$\dot{m}_r + \dot{m}_c = \dot{m}_T \tag{10}$$

$$\Delta P_c = \frac{1}{2}\rho V_c^2 \frac{f_c}{D_{ec}} \tag{11}$$

$$\Delta P_r = \frac{1}{2}\rho V_r^2 \frac{f_r}{D_{er}} \tag{12}$$

where, subscript c and r represent the flow in the center hole and the flow around the control rod, respectively. D_{ec}, D_{er} are equivalent diameters of the center hole and the control rod hole, f_c and f_r are the friction factor's of the center hole and around the control rod flow path.

From this approximation, the local critical velocity of the vibration (transition from turbulent excitation to wake shedding) was determined to be 3.4 m/sec.

7. Conclusions

The simulation experiment of flow induced vibration for the RCCAs of PWR produces the following useful conclusions.

(1) The amplitude of the vibration is the largest at the sixth plate at which the velocity is the highest.

(2) The frequency is about 20-26 Hz which is same as that of the control rod natural frequency. This means that the vibration is closely related with resonance.

(3) The governing mechanism of the vibration is wake shedding at the guide plate.

(4) From mass balance and pressure drop equations, the approximate critical velocity was found to be 3.4 m/sec. For more accurate measurement of the critical velocity, more advanced velocity measurement technique is required. For this purpose, the Particle Image Velocimetry (P. I. V.) may be used.

(5) For the reduction of control rod fretting wear by F. I. V. the bypass flow reduction is strongly recommended by the redesign of upper support plate to narrow the gap.

Acknowledgement

This research is supported by Electrical Engineering and Science Research Institute (E. E. S. R. I.). Especially the authors would like to acknowledge valuable technical comments from Engineer Byoung-young Choi and Taesik Lee.

References

Blevins, Robert D., 1997, "Flow-induced vibration," 0-442-20828-6.

Kim Kyung-Suk, Jung, Hyun-Chul, Kang, Ki-Soo, Kang, Young-June, Cha, Yong-Hoon and Jung, Woon-Gwan, 1999, "Experimental Analysis of Vibration Modes of Plates Using ESPI," *KSME International Journal*, Vol. 13, pp. 677~686.

Kim Sang-nyung and Shin Cheol, 1998, "Thermal Hydraulic Analysis for RCCA Fretting Wear caused by Flow-induced Vibration," *Korean Nuclear Society Spring Meeting*, Vol. 1, pp. 489~495.

Korea Energy Research Institute Material Corrosion Lab. 1997, "Technical Development of

RCCA Diagnosis," Intermediate Report.

Leclercq, J., 1995, "Mechanical Behaviour of Control Rod of 900 MWe PWR," Report No. RC/1-Revision 0.

Paidousis, M. P., 1981, "Fluidelastic Vibration of Cylinder Arrays in Axial and Cross Flow : State of the Art," *Journal of Sound and Vibration* (A81), 76(3), pp. 329~360.

Rho, Byung-Joon and Oh, Je-Ha, 1995, "LDV Measurement of Turbulent Flow Behavior of Droplets in a Two-Phase Coaxial Jet," *KSME Journal*, Vol. 9, pp. 360~368.

Ulchin Nuclear Center Plant Technical Team, 1995, "RCCA Inspection Follow-up Measures of Ulchin #1, 2 Plant," Wonbaldan(Noh) 743.06-Attachment.

Ulchin Nuclear Center Plant Technical Team, 1995, "RCCA Inspection Results," Ulchin #2 E. C. T. Experience.

Wambsganss, M. W. and Chen, S. S., 1971, "Tentative Design Guide for Calculating the Vibration Response of Flexible Cylindrical Elements in Axial Flow," *Argonne National Laboratory Report*, ANL-ETD-71-07.

Yasuo, A. and Paidoussis, M. P., 1989, "Flow-Induced Instability of Heat-Exchanger Tubes due to Axial Flow in a Diffuser-Shaped, Loose Intermediate Support," *Journal of Pressure Vessel Technology*, Vol. 111, pp. 428~434.